FEBS Letters 580 (2006) 3083–3090

Thermodynamics and stability of the PAAD/DAPIN/PYRIN domain of IFI-16

Kush Dalal, Frederic Pio*

Department of Molecular Biology and Biochemistry, Simon Fraser University, 8888 University Drive, Burnaby, BC, Canada V5A 1S6

Received 28 February 2006; revised 19 April 2006; accepted 20 April 2006

Available online 27 April 2006

Edited by Miguel De la Rosa

Abstract The PAAD domain is a conserved domain recently identified in more than 35 human proteins that are involved in apoptosis and inflammatory signaling pathways. Structural studies have confirmed that this domain belongs to the death domain superfamily which includes PAAD/CARD/DED/DD families. Recently, the 3D structures determined by NMR of NALP1 and ASC PAAD domain, members of the PAAD family, have shown that it is composed of a 6 helix bundle as with other death domain family members. However, helix-3 in the solved structures is unordered in solution. In this study we compare the thermodynamic, folding and stability properties of different members of the PAAD and CARD families and investigate structural conformational changes induced by the helix inducers trifluoroethanol and SDS on the PAAD domain of IFI16 and on the CARD domain of RAIDD. We show that inside the PAAD and CARD families, members have similar thermodynamic properties, however, the ΔG of folding for PAAD and CARD members are, respectively, -1.4 and -5.5 kcal mol^{-1}. This difference is attributed to less alpha helical content for PAAD due to the unfolding of helix-3 that lowers bonded energy and increases disorder when compared to CARD members. Despite identical fold between PAAD and CARD families but limited sequence identity, there are striking differences in the thermodynamics of both families.

Keywords: PAAD/DAPIN/PYRIN; Thermal denaturation; Circular dichroism; Protein stability; Fluorescence

1. Introduction

IFI16 has been identified as a target gene of interferon-γ and is a member of the HIN-200 gene family [1] that were initially grouped together based on their hematopoietic expression pattern, interferon inducibility, nuclear localization and common domain of 200 amino-acids repeat (HIN-200) of unknown structure and function. IFI16 acts as a transcription repressor when positioned in proximity to a promoter containing consensus binding sequences [2]. Each of the 200 amino-acids repeat regions contains this repression activity independently but seems to be enhanced by the N-terminus of IFI16 that can bind to DNA [2]. A nuclear function of IFI16 has been postulated by the findings that IFI16 and its mouse homolog p202 interact with nuclear factors p53, Rb, E2F, AP1, and NFκB proteins [3]. More recently, the PAAD/DAPIN/PYRIN domain, an apoptotic domain found at the N-termini of cell death and inflammatory proteins such as PYRIN, ASC, and AIM has been found in the N-terminus of IFI16, suggesting that IFI16 has a role in apoptosis and inflammation [4].

Structural studies have confirmed that this domain belongs to the death domain superfamily which includes PAAD/CARD/DED/DD families [4]. Recently, the 3D structures of the PAAD domains determined by NMR of NALP1 and ASC have shown that it is composed of a 6 helix bundle that fold as a Greek key topology as with other death domain family members. However, helix-3 in the solved structures is unordered in solution [5,6].

So far thermodynamics studies on the death domain fold has been poorly studied and recent studies have suggested as expected for a small domain of only 95 amino-acids that the death domain family members fold as a two-state equilibrium process with some differences in kinetics [7–14]. Only two folding kinetics studies have been performed on the CARD domain of RICK a pro-inflammatory serine threonine kinase and the pro-domain of caspase-1 [9,10]. These studies showed that both proteins are marginally stable with a free energy of folding of −1.1 kcal/mol for the prodomain of caspase-1 and −3 kcal/mol for RICK. Both proteins fold by an apparent two-state equilibrium process. Therefore, these proteins seem to fold slowly with different half-time and folding intermediates that can be kinetically trapped [9,10].

These data could indicate that folding pathways are not conserved within the structural superfamily. However, the differences between the folding kinetics of the different members of the superfamily remain to be established.

In this study, we compared the thermodynamic properties of many CARD and PAAD family by fluorescence and circular dichroism measurements. In addition, to investigate structural changes that could occur during folding–unfolding transition of CARD and PAAD domains we measured folding, thermodynamics and stability of two different death domains family members IFI16-PAAD and RAIDD-CARD using TFE and SDS helix inducers. These compounds have been used extensively for their ability to trap folding intermediates during folding–unfolding transition studies.

2. Material and methods

2.1. Cloning expression and purification of PAAD and CARD domains

Human DNA fragments encoding for PAAD protein domains of IFI16 referred to as IFI16-1 (3–88, CAI15085), NAC, (2–92, AAG30288), MNDA, (3–88, CAH73797) and CARD protein domains

*Corresponding author. Fax: +1 604 291 5583.
E-mail address: fpio@sfu.ca (F. Pio).

0014-5793/$32.00
doi:10.1016/j.febslet.2006.04.056

of RAIDD referred to as RAIDD-CARD (1–92, GI:4388927) and NAC referred to as NAC-CARD (1373–1473, AAG30288) were inserted into a pET28b vectors to produce a construct of each protein domain. Each protein domain was expressed as a His6-fusion protein in *Escherichia coli* BL21 (DE3) transformed with its respective construct. Proteins were purified according to the QIA-expressionist protocol (Qiagen). The proteins were eluted in the lysis buffer containing 250 mM imidazole then dialysed promptly in solubility buffer overnight to avoid precipitation. The PAAD domain of IFI16 was dialyzed against 50 mM sodium acetate, pH 4.0, while all other proteins were dialyzed against 50 mM Tris–HCl, 100 mM NaCl, pH 8.0. After dialysis all purified proteins were concentrated to approximately 10 mg/ml using an Amicon Ultra centrifugation filter with a 5000 dalton molecular weight cut off and then stored at −80 °C.

2.2. Limited proteolysis

A 2.1 mg/ml purifed IFI16-1 in 100 mM sodium acetate, pH 4.0, and 100 mM NaCl was digested with pepsin for 2 h at room temperature using an enzyme-to-substrate ratio of 1:30 (w/w). An identical IFI16-1 without added enzyme was subjected to the same incubation time at room temperature and used as a control to assess the extent of proteolysis by SDS–PAGE and MALDI-TOF MS. Following the incubation, the proteolytic reaction was stopped with 20 mM phenylmethanesulfonyl fluoride (PMSF). From this study a shorter construct named as IFI16-2 that contained the PAAD domain was obtained for further biophysical experiments.

2.3. MALDI-TOF MS experiment

Mass spectra were acquired on a Maldi TOF mass spectrometer (Perseptives Biosystems, Voyager). The matrix was a 10 mg/ml solution of α-cyano-4-hydroxycinnamic acid (CHCA); 10 mg of CHCA were dissolved in 400 μl deionized water, 100 μl 3% TFA and 500 μl acetonitrile. 1 μl of protein sample (900 μM) was mixed with 9 μl of matrix solution to a final concentration of 90 μM; 1 μl of the mixture was spotted on the sample plate. Once the samples had been dried at room temperature, the plate was transferred into the mass spectrometer for data collection. Deflection of low-mass ions was used to enhance the target protein signal.

2.4. Circular dichroism

CD spectra of PAAD and CARD domains were acquired on a JASCO J-810 spectropolarimeter equipped with a peltier type PFD-425S constant temperature cell holder. Both far and near UV spectra were converted into mean residue ellipticity and expressed in units of deg cm $dmol^{-1}$. Far UV measurements were made between 190 and 260 nm at 25 °C using a quartz cell with 0.05 cm light path length. Data were recorded using 200 nm/min scan rate, 100 mdeg sensitivity and 0.1 s response. The concentration of protein used was between 40 and 45 μM, depending on the protein studied. A baseline was subtracted from all spectra. Secondary structure content of each PAAD or CARD proteins were determined by the *cdPRO* program (http://lamar.colostate.edu/~sreeram/CDPro/main.html) using the CDSSTR algorithm, which gave the most accurate α-helix predictions of proteins with known structures. The percent α-helix reported is the sum of the regular plus disordered helix shown in the output of the *cdPRO* program. Near UV measurement between 400 and 250 nm were taken the same way as far UV, but in a 1 cm pathlength cuvette and at a protein concentration of 69–103 μM. Far and near UV measurement were taken in 6 M guanidine hydrochloride containing buffer to confirm loss of secondary and tertiary structure.

2.5. Fluorescence

Measurements were performed using the total fluorescence detector on the Jasco J-810 spectropolarimeter, or on a SLM 4800 spectrofluorimeter equipped with a single wavelength monochromator.

2.6. Chemical denaturation

Purified PAAD and CARD domains at 0.04 mg/ml were denaturated at different concentrations [0–7 M] of guanidine hydrochloride overnight at room temperature. At each guanidine hydrochloride concentration, the dichroic signal was measured for 30 s at 222 nm in a 10 mm quartz cell at 100 mdeg sensitivity and 0.1 s response at 298 K.

2.7. Thermal denaturation

PAAD and CARD domains at 0.04 mg/ml were denatured thermally and monitored by circular dichroism at 222 nm to detect the loss of α-helical content. The data were recorded using a 10 mm quartz cell, 100 mdeg sensitivity and 0.1 s response at 1° intervals. An attached peltier type constant temperature unit was used to heat the protein sample within the CD spectrophotometer from 20 to 100 °C. In the case of the PAAD domain of IFI16, the renaturation spectra was also obtained by performing the reverse scan from 100 to 20 °C just after denaturation by heating.

2.8. Analysis of denaturation curves

Thermodynamic parameters were obtained by using the linear extrapolation model [15,16]. In all cases the denaturation was assumed to follow a two-state model

$$\mathrm{N} \leftrightarrow \mathrm{D},$$

where N is the native state and D is the denatured state. At any point during the denaturation, the sum of the fractions of native and denatured proteins $f_D + f_N = 1$. This is determined by making extrapolations of the linear portions of the protein denaturation curve in the native and denatured regions, y_N and y_D, respectively, such that the experimentally observed

$$y_{OBS} = y_N f_N + y_D f_D. \quad (1)$$

When substituting $f_D = f_N - 1$ and $f_N = f_D - 1$ in Eq. (1), $f_D = (y_{OBS} - y_N)/(y_D - y_N)$ and $f_N = (y_D - y_{OBS})/(y_D - y_N)$. Since the equilibrium constant $K_D = f_D/f_N = (y - y_N)/(y_D - y)$, the ΔG_D at each point in the denaturation can be determined with the expression.

$$\Delta G_D = -RT \ln(K), \quad (2)$$

where R is the gas constant, T is the temperature in Kelvin and K is equilibrium constant K_D.

For the chemical denaturation of PAAD and CARD domains, The ΔG_{H20}, or the free energy of folding in the absence of denaturant, was determined by plotting

$$\Delta G_D = -RT \ln(K) = \Delta G_D^{H20} - m(\text{denaturatant}), \quad (3)$$

assuming a linear dependence of ΔG_D on denaturant concentration. The ΔG_{H20} is the Y axis intercept, the [denaturant] is the molar guanidine hydrochloride concentration and m is the slope of the curve ΔG_D over the molar guanidine hydrochloride concentration.

For the temperature denaturation of PAAD and CARD domains a Van't Hoff analysis was performed by plotting $\ln(K_D)$ against 1/K. The ΔH values were calculated from the plots as $\Delta H = \text{slope} \times R$ ($R = 1.987 \times 10^{-3}$ kcal/mol K). The variation in entropy was calculated according to $\Delta S = \Delta H/T_m$ where T_m is the temperature at the midpoint of the unfolding transition. With these parameters, the $\Delta G_{folding}$ at 298 K was determined by the expression

$$\Delta G_{folding} = \Delta H - T\Delta S. \quad (4)$$

The actual computation of thermodynamic parameters for thermal denaturations performed in this study was done using the Jasco Spectra Analysis software version 1.53.04 [Build 1].

2.9. Homology modeling

To perform homology modeling, we chose the PAAD template from NALP1 (PDB code 1PN5) and aligned the IFI16-PAAD domain sequence to NALP1 using the multiple alignment of [6] as a basis then refined the alignment further manually. Finally the model were built and/or refined with the program MODELLER [17]. Two non-default key parameters of MODELLER were used during model building and refinement. First, extensive loop modeling was enabled (via the DO_LOOPS option). This option increases the quality of the model in the loop regions. Second, molecular dynamics with simulated annealing was enabled (via MD_LEVEL = 'refine1'). This option further improves the overall energy and quality of the model by exploring a larger conformational space and obtaining models with the lowest global energy. The model were checked for favorable threading energy and geometrical and stereochemical properties using Verify3D [18] and PROCHECK [19].

3. Results

3.1. Spectroscopic properties of IFI16-PAAD

IFI16-1 has 3 tyrosines and 3 phenylalanines and no tryptophan. The tyrosine fluorescence emission spectra obtained at 275 nm excitation of native and denaturated protein shows the characteristic maximum of tyrosine at 304 nm (Fig. 1). The decrease in relative fluorescence intensity observed in 6 M guanidine hydrochloride containing buffer indicating that the tyrosines become accessible to solvent upon unfolding and suggest that the environment of the chromophores changes and the protein contains tertiary structure. The phenylalanine emission spectrum at 260 nm excitation wavelength shows a single peak with a maximum at 304 nm that corresponds to tyrosine but with less intensity than when excited at 280 nm. Since no peak corresponding to phenylalanine in the emission spectrum is observed at 282 nm we suggest that the low phenylalanine fluorescence intensity is further weakened by the possible chromophores location in the disordered region of the protein or their exposure to solvent in the tertiary structure of IFI16. Furthermore, consistent with this explanation, the fluorescence intensity in the phenylalanine emission spectrum is also completely attenuated in 6 M guanidine hydrochloride containing buffer. To confirm that there are no tryptophan contaminants in our sample, the emission spectrum at 295 nm excitation wavelength was recorded. The results show the absence of the typical tryptophan peak at 353 nm and single peak at 304 nm, indicating only tyrosine emission. This is consistent with a pure protein sample as confirmed by SDS–PAGE analysis after silver staining. No differences were observed in the spectroscopic properties of IFI16-1 when further purified by cation-exchange chromatography.

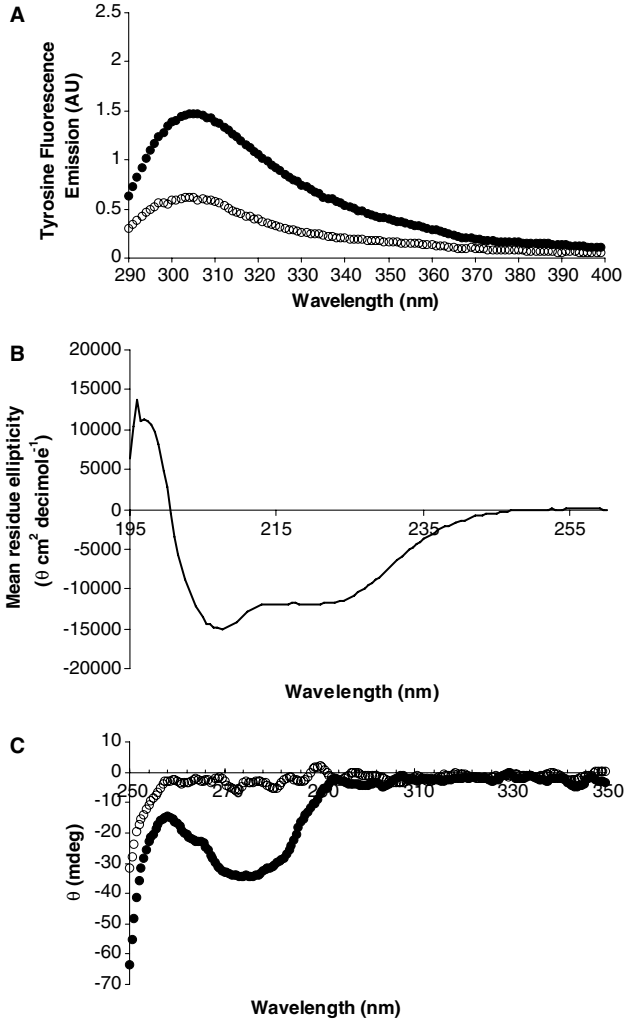

Fig. 1. Spectroscopic properties of the PAAD domain of IFII6. (A) Tyrosine fluorescence emission. (B) Far UV circular dichroism spectrum. (C) Near UV circular dichroism spectrum. (●) native conditions (○) denaturating conditions (6 M guanidine hydrochloride).

We further characterized IFI16-1 by far and near-UV circular dichroism. Far UV circular dichroism spectra (Fig. 1B) show well defined minima at 208 and 222 nm confirming the highly helicoidal content of the protein. The far UV spectra of IFI16 were not affected by additive purification steps suggesting that HIS-Tag purification was sufficient for circular dichroism analysis. The far UV spectra of IFI16-1 at pH 4.0–5.5 are superimposable upon each other suggesting that secondary structure is pH independent in the range tested. The near UV spectrum of IFI16-1 shows a minimum at 275 nm corresponding to tyrosine and confirms that aromatic amino-acids are packed in an asymmetric environment. The near UV spectra (Fig. 1C) after denaturation in 6 M urea shows a decrease in signal intensity indicating that the aromatic amino-acids are buried in the native structure. Taken together, these data demonstrate that IFI16-1 is well folded with both secondary and tertiary structure.

3.2. Modeling and secondary structure of the IFI16-PAAD domain

PAAD proteins share low sequence similarities (~15%) except for MNDA and IFI16-PAAD which share 50% sequence identity. In spite of this low sequence identity the two published structures of PAAD domains from NAC and ASC are both six helix bundles with a disordered helix-3 [5,6]. For these reasons we modeled the PAAD domain of IFI16 by homology modeling (Fig. 2) using the NMR structure of NALP1-PAAD domain as a template (pdb code:1PN5). The model has 51 residues incorporated into α-helix which is 40.5% of the total 126 amino-acids in the expressed protein. To confirm the unfolding of the helix-3 of IFI16-1 we measured the total amount of α-helix using far UV circular dichroism spectra and analyzed the helical content using cdPRO. Our results show 40.3 ± 1.2% α-helix, which is 99.5% consistent with the calculated α-helix secondary structure from the model. Similar analysis for RAIDD-CARD and NAC-PAAD domains using their respective published NMR structures [20,5] indicate 97.3% for RAIDD-CARD and 91% for the NAC-PAAD of the calculated α-helix secondary structure from their respective models. These data are consistent with a disordered helix for the PAAD domain of IFI16.

3.3. Thermodynamic properties of the IFI16-PAAD domain

Thermodynamic parameters for IFI16-PAAD were obtained by analyzing denaturation curves that were recorded by monitoring either far UV-CD signal or total fluorescence of tyrosine residues (Table 1). All curves were fitted to a two-state equilibrium folding model [15]. The free energy of folding, $\Delta G^{25\ \mathrm{degC}}_{\mathrm{folding}}$, obtained by circular dichroism and fluorescence were -1.40 ± 0.392 and -2.04 kcal/mol, respectively when the

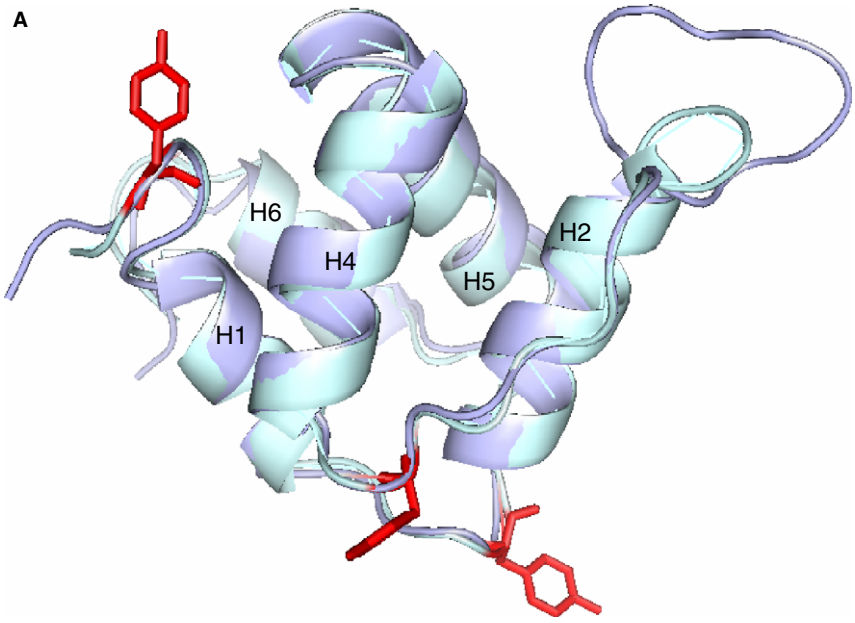

Fig. 2. Homology modeling of the PAAD domain of IFI16 on NALP1. (A) Superimposition of NALP1-PAAD domain (purple) (pdb code:1PN5) with the IFI16-PAAD model generated with Modeller software (light blue) (RMSD = 0.88 Å). All the tyrosine in the IFI16 model are colored in red. (B) sequence alignment of the PAAD domain of NALP1 with IFI16 from which the model was generated. Amino-acids colored in grey are conserved between IFI16-PAAD and NALP1.

Table 1
Thermodynamic parameters for thermal and chemical unfolding transition of PAAD and CARD domains

Protein	$\Delta G^{25\ degC}_{folding}$ (kcal mol^{-1})	$\Delta G^{25\ degC}_{H20}$ (kcal mol^{-1})*	ΔH (kcal mol^{-1})	ΔS (kcal mol^{-1} K^{-1})	T_m (°C)	m (kcal mol^{-1} M^{-1})	C_m(M)	ΔASA (Å^2)
PAAD								
IFI16-1[a]	−1.40 ± 0.392	−1.75	−24.80 ± 2.16	−0.079 ± 0.0060	42.05 ± 3.99	−1.70	1.03	3822
IFI16-2[a]	−2.77 ± 0.236	−2.13	−34.37 ± 2.16	−0.106 ± 0.0065	51.51 ± 0.516	−1.89	1.12	4686
NAC	−1.46	–	−23.67	−0.074	44.72	–	–	–
MNDA	−3.68 ± 1.20	−1.43	−49.43	−0.151	55.09	−1.02	1.40	732
CARD								
RAIDD	−5.28	−4.09	−55.37	−0.168	57.39	−2.30	1.78	5322
NAC	−5.796	−3.35	−54.64	−0.164	60.38	−1.89	1.77	4686
RICK[b]	–	−3.0 ± 0.15	–	–	–	−1.24	2.4	8200
CPI[b]	–	−1.1 ± 0.2	–	–	–	−0.69	1.7	2780

[a]Average values over pH range 4.0–5.5.
[b]Values obtained by urea denaturation according to [9,10].

linear extrapolation model was used to analyze denaturations curves. If the three tyrosine amino-acids present in IFI16-1 are in distinct chemical environments, the variation in $\Delta G^{25\ degC}_{folding}$ observed could be explained by the different accessibility to solvent of each tyrosine during melting. The two thermal denaturation curves were not superimposable upon one another, but the extrapolated ΔH and ΔS values were almost identical.

To investigate the reversibility of the folding–unfolding transition of the PAAD domain of IFI16, the sample was renaturated after thermal denaturation followed by circular dichroism (Fig. 3). When IFI16-1 was denatured and then renatured, the T_m values were nearly identical and the unfolding–refolding curves superimposed well upon each other when expressed in fraction unfolded. The results confirm that refolding of IFI16-1 into the native state is possible and that the unfolding process occurs by a two-state mechanism.

The IFI16-1 conformational stability obtained from chemical denaturation, ΔG^{H20}, was −1.7 kcal/mol when guanidine hydrochloride was used as the denaturant (Table 1). The corresponding m value and Gdn-HCl$_{1/2}$ (C_m) were 1.7 kcal/mol/M and 1.03 M. The m value has been shown to correlate with

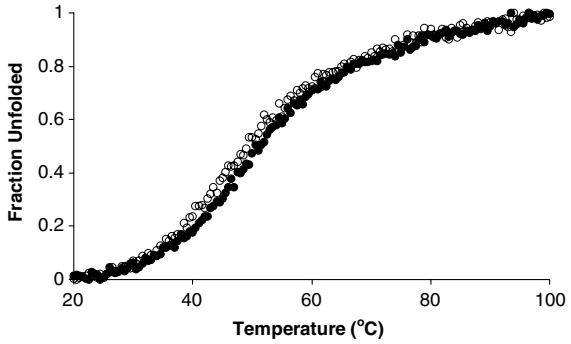

Fig. 3. Thermal reversibility of IFI16-1. Superimposed IFI16-1 (●) denaturation and (○) renaturation curves over 20–100 °C.

the amount of surface area exposed upon denaturation and the total number of residues in the protein [16]. We determined the change in accessible surface area (ΔASA) to be 3822 Å^2, which corresponds to a 51 residue protein. This does not agree with the IFI16-1 length of 126 residues, which should give a ΔASA of 10811 Å^2 but agree with the model of the IFI16-1 that shows 51 residues folded into α-helix. The surface area already exposed within the disordered region that include helix-3 contribute to the 6989 Å^2 difference. The *m* value can also be lower than expected if the protein has more than two equilibrium states during unfolding [15]. Furthermore, IFI16-1 has a highly positive charge since it was tested at pH 4.0 and has a p*I* of 9.72. The repulsions of positive charges can cause extension of unfolded proteins, which increases the accessibility to solvent and lowers the *m* value and ΔASA [16]. Overall, thermal and chemical denaturation shows that IFI16-1 has low stability, high conformation entropy and low bonded energy.

Compact and folded regions of proteins are generally less sensitive to proteases than exposed and disordered regions. Limited proteolysis has been widely used to improve the conformational stability of proteins [21] and eventually improve the crystallizibility of macromolecules. Since IFI16 is soluble and well folded between pH 4.0 and 5.5, we identified proteases that function in acidic conditions. Partial digestion by pepsin of IFI16 were performed at different molar ratios of protein:enzyme (1:0 → 1:6) and stopped by adding PMSF after 20 min. Protein fragments were analyzed on an 18% SDS–PAGE gel to monitor the extent of proteolysis. Once the partial digestion conditions were obtained, the digestion mixture was analyzed by MALDI-TOF mass spectrometry. Fragment analysis by FindPept (www.expasy.org) identified a cleavage site 5 residues away from the N terminus which was accessible to proteolytic cleavage. This truncated protein, designated IFI16-2, was cloned, expressed and found to have the same solubility properties as IFI16-1. Secondary structure, tertiary structure and thermodynamics were analyzed the same way as IFI16-1 (Table 1). The IFI16-2 $\Delta G^{25\ degC}_{folding}$ was found to be −2.77 ± 0.236 kcal/mol, which is almost double the conformational stability of IFI16-1. When guanidine hydrochloride was used to denature IFI16-2, the ΔG^{H20} was found to be −2.13 kcal/mol, which is lower than the corresponding IFI16-1 value. The *m* value and Gdn-HCl$_{1/2}$ (C_m) were −1.89 kcal/mol/M and 1.12 M, respectively. As with IFI16-1 the ΔASA for IFI16-2 was calculated using the *m* value and found to be 4686 Å^2, which corresponds to a 60 residue protein. This does not agree with the 118 amino-acid length of IFI16-2. The reasons for the lower than expected *m* value is the same as mentioned above for IFI16-1. The CD spectra of IFI16-2 show higher helicoidal content and significant tertiary structure since we observe lower minima at 222 and 208 nm in far UV spectra, and a lower minimum at 275 nm (tyrosine) in near UV spectra compared to IFI16-1.

3.4. IFI16-PAAD compared to other PAAD and CARD domains

We compared the thermodynamic properties of IFI16-1 and IFI16-2 to other members of the Death Domain superfamily. Thermal and chemical denaturations were performed on NAC-PAAD (NALP1), MNDA-PAAD, NAC CARD and RAIDD-CARD (Table 1). CD and fluorescence emission spectra were recorded for all proteins to confirm secondary and tertiary structure before acquiring denaturing data (Fig. 4). The average ΔG^{H20} and $\Delta G^{25\ degC}_{folding}$ for PAAD domains (IFI16, NAC, MNDA) were −1.77 ± 0.36 and − 2.33 ± 1.10 kcal/mol, respectively. CARD domains have greater stability than PAAD domains as seen from their average ΔG^{H20} and $\Delta G^{25\ degC}_{folding}$ values of 2.89 ± 1.27 and 5.54 ± 0.36 kcal/mol, respectively. For the ΔG^{H20} of CARD domains we included denaturation data on RICK-CARD and CPI-CARD (procaspase 1) which were characterized by equilibrium unfolding studies using urea [9,10]. The denaturation curves should be

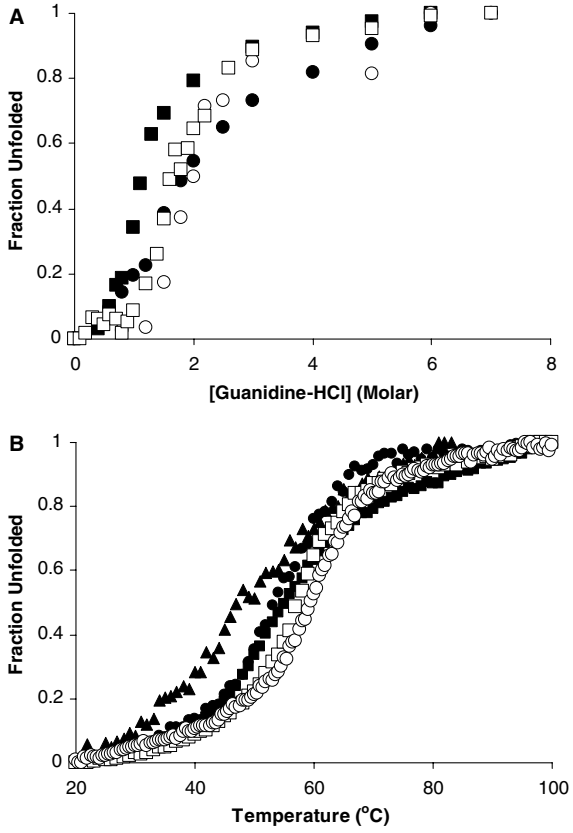

Fig. 4. Thermal and chemical denaturation show PAAD domains are less stable that CARD domains. PAAD and CARD proteins were denatured by (A) guanidine hydrochloride or (B) temperature at a concentration of 0.04 mg/mL and monitored by circular dichroism at 222 nm. (▲) NAC PAAD (T_m = 44.7 °C); (●) MNDA PAAD (T_m = 55.0 °C); (■) IFI16-1 (T_m = 42.1 °C); (□) RAIDD-CARD (T_m = 57.4 °C); (○) NAC-CARD (T_m = 60.4 °C).

similar when the linear extrapolation model is used [15]. Furthermore, the m values of urea and guanidine hydrochloride for many proteins correlate with each other with an R value of 0.9 [16]. Thus, we are confident that the ΔG^{H20} data for RICK-CARD (-1.1 ± 0.2 kcal/mol) and CPI-CARD (3.0 ± 0.15 kcal/mol) can be compared directly to our guanidine hydrochloride derived values.

CARD domains show considerably more variation in ΔG^{H20} values than PAAD domains. Both RICK-CARD and CPI-CARD have low stability, which increases the overall deviation for CARD domains. In the case of PAAD domains, the ΔG^{H20} values are more consistent than CARD domains with only a 0.36 kcal/mol standard deviation between the 3 proteins tested. In spite of this, the relative conformation stability for CARD domains is higher than for PAAD domains, which is in agreement for average $\Delta G^{25\ degC}_{folding}$ values obtained from analysis of thermal denaturation curves.

3.5. Increasing secondary structure with helix inducers

Sodium dodecyl sulphate (SDS) and 2,2,2-trifluoroethanol (TFE) were used for helix induction of IFI16-1 and IFI16-2. Each sample of protein was manually prepared to contain the desired SDS:protein molar ratio and analyzed by far-UV CD to determine secondary structure content. All SDS concentrations used were below the critical micelle concentration (CMC) of approximately 8 mM. Fig. 5A shows that at low molar ratios of SDS:protein (5:1 → 60:1), IFI16-1 and IFI16-2 adopt an unfolded state suggested by the loss of the 208 nm peak and by cdPRO analysis of the far-UV spectra. In the SDS induced unfolded state, the peak at 208 nm becomes positive, which represents a $\pi \rightarrow \pi^*$ shift in polarity in the amide portion of the peptide backbone. At intermediate SDS:Protein molar ratios (60:1 → 160:1), the protein regains helicity reach a maximum value at approximately 160 SDS:1 protein for IFI16-1 and 120 SDS:1 protein for IFI16-2. When the SDS content was increased beyond this point, the secondary structure content was decreased for both proteins. The cdPRO analysis of far UV spectra for both proteins IFI16-1 and IFI16-2 with SDS show a 7% increase in helical content at the maximum SDS:protein molar ratio compared to protein with no SDS, which corresponds to the refolding of helix-3. In the refolded state, the peak at 208 nm has greater intensity. In contrast, the peak at 222 nm, which represents the $n \rightarrow \pi^*$ electronic transition, remains stable. In conjunction, we did not observe an increase in helicity at any SDS concentration for the CARD domain of RAIDD, which contains 6 folded helices (Fig. 6).

Thermal denaturation for IF116-1 and IFI16-2 were performed in the presence of SDS to test if the increases in helicity were accompanied by a greater stability of the protein (Fig. 5B). For the SDS concentrations at which greater folding of IFI16-1 is obtained, we observe a $\Delta G_{folding}$ of -7.2 kcal mol^{-1} for

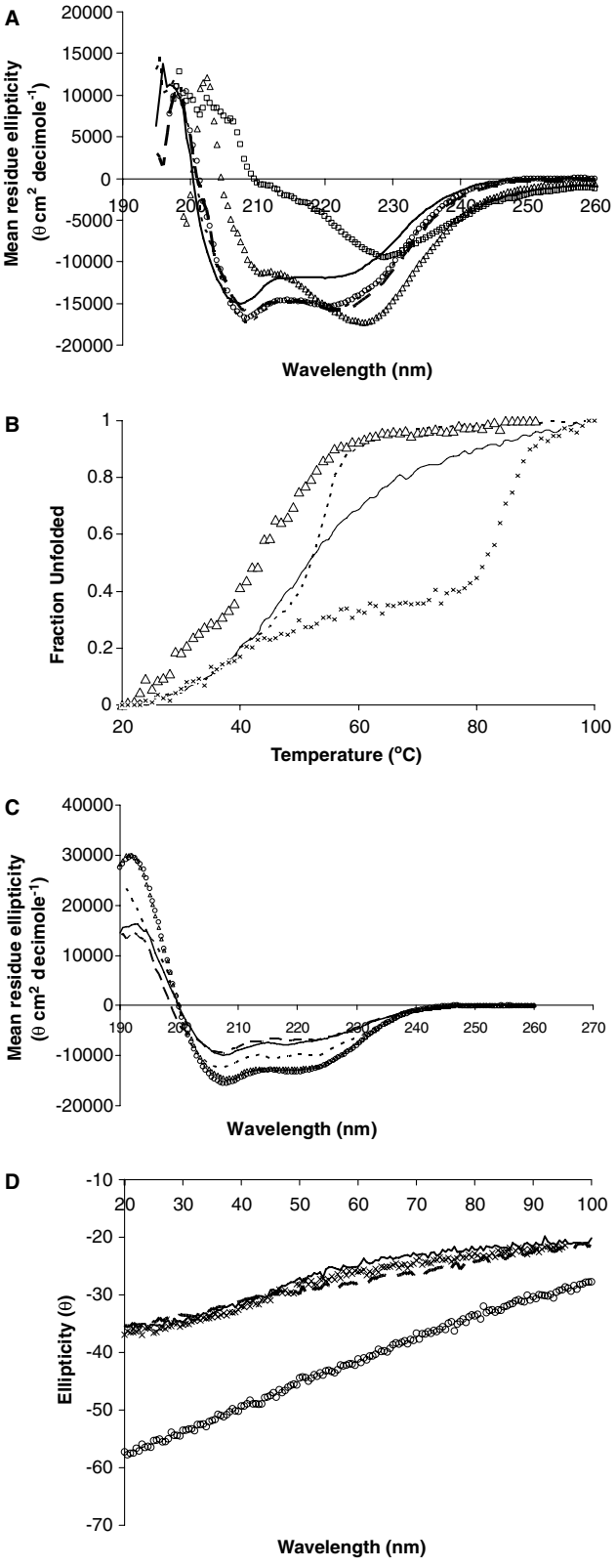

Fig. 5. Both helix secondary structure and stability of IFI16-1 are improved in an amphipathic environment. (A) The helical content of IFI16-1 at 2.76 μM measured by far UV CD in the presence of increasing SDS concentrations: (solid line) No SDS; (□) 110 μM SDS; (△) 221 μM SDS; (– –) 331 μM SDS; (--) 441 μM SDS; (○) 551 μM SDS. (B) Thermal denaturation of IFI16-1 at 2.76 μM monitored by CD at 222 nm in the presence of increasing SDS concentrations: (solid line) No SDS; (△) 221 μM SDS (--) 441 μM SDS (×) 1.3 mM SDS. (C) The helical content of IFI16-PAAD at 2.76 μM in the presence of increasing TFE concentration: (solid line) No TFE; (– –) 5% TFE; (--) 20% TFE; (○) 30% TFE; (△) 40% TFE. (D) Thermal denaturation of IFI16-1 monitored by CD at 222 nm in TFE: (solid line) No TFE; (×) 1% TFE; (--) 5% TFE; (○) 30% TFE.

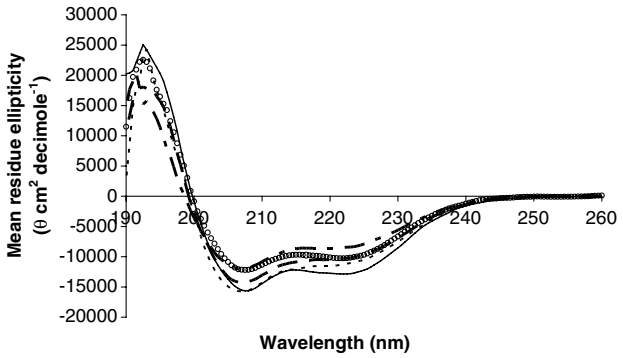

Fig. 6. RAIDD-CARD helicity does not increase at any SDS concentration. Secondary structure of RAIDD-CARD at 3.2 μM in the presence of SDS measured by far UV CD: (solid line) No SDS; (– –) 176 μM SDS; (---) 352 μM SDS; (– -) 704 μM SDS; (○) 1.06 mM SDS.

IFI16-1 and −6.5 kcal mol^{-1} for IFI16-2 which is considerably higher than their corresponding $\Delta G_{folding}$ without SDS in Table 1 (IFI16-1, −1.43 kcal mol^{-1}; IFI16-2, −2.77 kcal mol^{-1}). The thermal denaturation curves at SDS concentrations at which PAAD domains were unfolded had lower T_m values than protein without SDS, did not follow a two-state transition and hence, could not be analyzed by linear extrapolation. At SDS concentrations beyond the unfolded and refolded states, both IFI16-1 and IFI16-2 are very stable with T_m values approximately of 90 °C when a molar ratio of 480 SDS:1 protein was applied. Due to the irregularity of these curves at high SDS concentrations, they also could not be analyzed by linear extrapolation.

TFE was also used to promote helix formation of IFI16-1. As with the SDS titration, each sample of protein was prepared to contain the desired TFE concentration before CD analysis. We show that TFE increases secondary structure with increasing concentration from 0% to 30% volume/volume (Fig. 5C). No further increase in helical contents were observed after this concentration. These data suggest that the partially folded PAAD domain allows propagation of secondary structure due to water molecules exchange by TFE. No further helicity is gained beyond 30% TFE. When 1% TFE is added (Fig. 5D), the thermal denaturation show loss of a two-state unfolding mechanism, suggesting a collapse of the tertiary structure of IFI16-1 at low concentration of TFE.

4. Discussion

The comparison of the thermodynamic parameters between CARD and PAAD family members shows that there are intrinsic differences between both families. CARD family members are more stable with less conformational entropy and more bonded energy than PAAD family members, consistent with the fact that the PAAD domain is partially folded. In addition, there are striking differences between members of the same family, suggesting that the death domain has a more or less compact three-dimensional structure that allow it to recognize different binding partners with different protein affinities.

The water miscible organic solvent TFE has been recognized as a model solvent for its ability to propagate α-helix by replacing water molecules bound to the peptide backbone by TFE molecules that modify dielectric constant of the medium. Intense helix formation has been found at high or low concentration of TFE. At low concentration there has been evidences suggesting that this propagation of secondary structure seems to be restricted by the tertiary structure of the protein. For IFI16-1, low concentration of TFE can increase secondary structure propagation probably due to the partially folded structure of IFI16 [22–27].

The different effect of SDS below the CMC at different concentration on the secondary structure and stability of IFI16-1 suggest that the SDS–protein ratio confer different conformational behaviour for IFI16-1. A structural model of protein–surfactant complex that involves SDS and protein has been suggested such as the protein wrap around the micelle or the micelle nucleate around the hydrophobic sites of the proteins (neck and beads model) [28]. These structures could account for different conformational behavior of the SDS–protein complex. However, both models can be ruled out in our experimental conditions, which are far below the CMC.

Acknowledgement: F.P. is grateful for the financial support provided by the Canadian Institute for Health Research (CIHR), Michael Smith Foundation for Health Research (MSFHR) and Alfred P. Sloan Foundation Strategic Training Program in Bioinformatics for Health Research. This work was also supported by grants from Canada's Natural Science and Engineering Council of Canada (NSERC) and British Columbia Advanced Systems Institute (ASI).

References

[1] Dawson, M.J. and Trapani, J.A. (1996) HIN-200: a novel family of IFN-inducible nuclear proteins expressed in leukocytes. J. Leukoc. Biol. 60, 310–316.
[2] Johnstone, R.W., Kerry, J.A. and Trapani, J.A. (1998) The human interferon-inducible protein, IFI 16, is a repressor of transcription. J. Biol. Chem. 273, 17172–17177.
[3] Min, W., Ghosh, S. and Lengyel, P. (1996) The interferon-inducible p202 protein as a modulator of transcription: inhibition of NF-kappa B, c-Fos, and c-Jun activities. Mol. Cell. Biol. 16, 359–368.
[4] Pawlowski, K., Pio, F., Chu, Z., Reed, J.C. and Godzik, A. (2001) PAAD – a new protein domain associated with apoptosis, cancer and autoimmune diseases. Trends Biochem. Sci. 26, 85–87.
[5] Hiller, S., Kohl, A., Fiorito, F., Herrmann, T., Wider, G., Tschopp, J., Grutter, M.G. and Wuthrich, K. (2003) NMR structure of the apoptosis- and inflammation-related NALP1 pyrin domain. Structure 11, 1199–1205.
[6] Liepinsh, E., Barbals, R., Dahl, E., Sharipo, A., Staub, E. and Otting, G. (2003) The death-domain fold of the ASC PYRIN domain, presenting a basis for PYRIN/PYRIN recognition. J. Mol. Biol. 332, 1155–1163.
[7] Bose, K. and Clark, A.C. (2005) pH effects on the stability and dimerization of procaspase-3. Protein Sci. 14, 24–36.
[8] Feeney, B., Pop, C., Tripathy, A. and Clark, A.C. (2004) Ionic interactions near the loop L4 are important for maintaining the active-site environment and the dimer stability of (pro)caspase 3. Biochem. J. 384, 515–525.
[9] Chen, Y.R. and Clark, A.C. (2003) Equilibrium and kinetic folding of an alpha-helical Greek key protein domain: caspase recruitment domain (CARD) of RICK. Biochemistry 42, 6310–6320.
[10] Chen, Y.R. and Clark, A.C. (2004) Kinetic traps in the folding/unfolding of procaspase-1 CARD domain. Protein Sci. 13, 2196–2206.
[11] Pop, C., Chen, Y.R., Smith, B., Bose, K., Bobay, B., Tripathy, A., Franzen, S. and Clark, A.C. (2001) Removal of the pro-domain does not affect the conformation of the procaspase-3 dimer. Biochemistry 40, 14224–14235.

[12] Pop, C., Feeney, B., Tripathy, A. and Clark, A.C. (2003) Mutations in the procaspase-3 dimer interface affect the activity of the zymogen. Biochemistry 42, 12311–12320.
[13] Bose, K. and Clark, A.C. (2001) Dimeric procaspase-3 unfolds via a four-state equilibrium process. Biochemistry 40, 14236–14242.
[14] Bose, K., Pop, C., Feeney, B. and Clark, A.C. (2003) An uncleavable procaspase-3 mutant has a lower catalytic efficiency but an active site similar to that of mature caspase-3. Biochemistry 42, 12298–12310.
[15] Pace, C.N. (1986) Determination and analysis of urea and guanidine hydrochloride denaturation curves. Methods Enzymol. 131, 266–280.
[16] Myers, J.K., Pace, C.N. and Scholtz, J.M. (1995) Denaturant *m* values and heat capacity changes: relation to changes in accessible surface areas of protein unfolding. Protein Sci. 4, 2138–2148.
[17] Sanchez, R. and Sali, A. (1997) Evaluation of comparative protein structure modeling by MODELLER-3. Proteins Suppl. 1, 50–58.
[18] Luthy, R., Bowie, J.U. and Eisenberg, D. (1992) Assessment of protein models with three-dimensional profiles. Nature 356, 83–85.
[19] Laskowski, R.A., Rullmannn, J.A., MacArthur, M.W., Kaptein, R. and Thornton, J.M. (1996) AQUA and PROCHECK-NMR: programs for checking the quality of protein structures solved by NMR. J. Biomol. NMR 8, 477–486.
[20] Chou, J.J., Matsuo, H., Duan, H. and Wagner, G. (1998) Solution structure of the RAIDD CARD and model for CARD/CARD interaction in caspase-2 and caspase-9 recruitment. Cell 94, 171–180.
[21] Cohen, S.L., Ferre-D'Amare, A.R., Burley, S.K. and Chait, B.T. (1995) Probing the solution structure of the DNA-binding protein Max by a combination of proteolysis and mass spectrometry. Protein Sci. 4, 1088–1099.
[22] Buck, M. (1998) Trifluoroethanol and colleagues: cosolvents come of age. Recent studies with peptides and proteins. Q. Rev. Biophys. 31, 297–355.
[23] Rajan, R. and Balaram, P. (1996) A model for the interaction of trifluoroethanol with peptides and proteins. Int. J. Pept. Protein Res. 48, 328–336.
[24] Luo, P. and Baldwin, R.L. (1997) Mechanism of helix induction by trifluoroethanol: a framework for extrapolating the helix-forming properties of peptides from trifluoroethanol/water mixtures back to water. Biochemistry 36, 8413–8421.
[25] Shiraki, K., Nishikawa, K. and Goto, Y. (1995) Trifluoroethanol-induced stabilization of the alpha-helical structure of beta-lactoglobulin: implication for non-hierarchical protein folding. J. Mol. Biol. 245, 180–194.
[26] Yang, J.J., Buck, M., Pitkeathly, M., Kotik, M., Haynie, D.T., Dobson, C.M. and Radford, S.E. (1995) Conformational properties of four peptides spanning the sequence of hen lysozyme. J. Mol. Biol. 252, 483–491.
[27] Sivaraman, T., Kumar, T.K., Hung, K.W. and Yu, C. (1999) Influence of disulfide bonds on the induction of helical conformation in proteins. J. Protein Chem. 18, 481–488.
[28] Guo, X.H., Zhao, N.M., Chen, S.H. and Teixeira, J. (1990) Small-angle neutron scattering study of the structure of protein/detergent complexes. Biopolymers 29, 335–346.